NANO LETTERS

Letter

pubs.acs.org/NanoLett

Biological Templates for Antireflective Current Collectors for Photoelectrochemical Cell Applications

Chia-Ying Chiang,[†] Jillian Epstein,[†] Adam Brown,[‡] Jeremy N. Munday,[§] James N. Culver,[‡,∥] and Sheryl Ehrman*[,†]

[†]Department of Chemical and Biomolecular Engineering, [‡]Institute for Bioscience and Biotechnology Research, [§]Department of Electrical and Computer Engineering, and [∥]Department of Plant Science and Landscape Architecture, University of Maryland, College Park, Maryland 20742, United States

Supporting Information

ABSTRACT: Three-dimensional (3D) structures such as nanowires, nanotubes, and nanorods have the potential to increase surface area, reduce light reflection, and shorten charge carrier transport distances. The assembly of such structures thus holds great promise for enhancing photoelectrochemical solar cell efficiency. In this study, genetically modified *Tobacco mosaic virus* (TMV1cys) was used to form self-assembling 3D nanorod current collectors and low light-reflecting surfaces. Photoactive CuO was subsequently deposited by sputtering onto these patterned nanostructures, and these structures were examined for photocurrent activity. CuO thicknesses of 520 nm on TMV1cys patterned current collectors produced the highest photocurrent density of 3.15 mA/cm^2 yet reported for a similar sized CuO system. Reflectivity measurements are in agreement with full-wave electromagnetic simulations, which can be used as a design tool for optimizing the CuO system. Thus the combined effects of reducing charge carrier transport distance, increasing surface area, and the suppression of light reflection make these virus-templated surfaces ideal for photoelectrochemical applications.

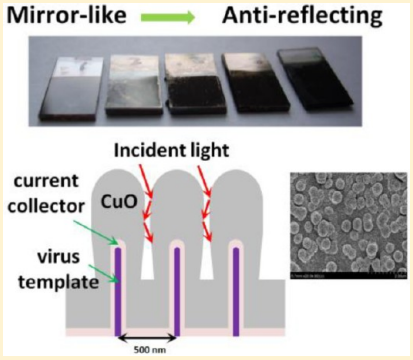

KEYWORDS: *Photoelectrochemical cell, self-assembled current collector, antireflective structure, CuO*

Currently, over 80% of the world's energy consumption is derived from fossil fuels.[1,2] However, this method of electrical generation has posed significant concerns regarding widespread environmental damage. A more sustainable alternative to fossil fuels was first presented by Fujishima and Honda when they successfully produced hydrogen from the photoelectrolysis of water using a TiO_2 semiconducting electrode.[3,4] Successful water electrolysis is achieved when the semiconducting electrode material absorbs photons with energy at or greater than its band gap, generating electron/hole pairs.[1,5−8] These electron/hole pairs are collected at the anode and cathode of the solar cell where they drive the redox reactions that produce hydrogen gas, along with the byproduct oxygen gas.[5,6] This solar cell, more specifically, is called a photoelectrochemical (PEC) cell.

Three major issues related to PEC cell efficiency are photon absorption, electron transport, and the redox potential of the water splitting reaction. Many studies have focused on the use of nanostructures to shorten the charge carrier transport distance by introducing three-dimensional (3D) nanowires, nanotubes, and nanorods.[9−11] However, only a few PEC studies have investigated the efficiency of utilizating incident light as a means to enhance PEC activity.[12,13] In particular, mimicking the structure of natural surfaces that contain periodic nanostructures such as those found in the eye of the moth represents a potentially useful means to decrease light reflection. This structure works because the nanostructures are smaller than the wavelength of visible light, and thus the light sees the surface having a continuous refractive index gradient between the air and the medium, which decreases reflection by removing the air−solid interface. With such a structure for eyes, moths can see very well in the dark without being captured by their predators because of the light reflection from their eyes. For the next generation solar cells, structures with a scale comparable to the wavelengths of the majority of the useful solar spectrum are the ideal design.[14]

There is growing interest in harnessing the self-assembly and inorganic binding capabilities derived from biological materials, especially the novel bioinorganic interfaces of the genetically tractable virus.[15−18] Subsequently, viruses have been used as scaffolds to produce novel bioinorganic interfaces that function as battery electrode materials, conductive nanowires, and memory devices.[18−20] In this study, a genetically modified *Tobacco mosaic virus* (TMV1cys) with a particle length of 300 nm and an outer diameter of 18 nm was patterned on a gold substrate to form nanoscaled 3D structures. The introduction of a cysteine residue within the virus coat protein enabled the patterning of TMV1cys onto metal substrates and enhanced

Received: September 26, 2012
Revised: October 23, 2012
Published: October 30, 2012

   dx.doi.org/10.1021/nl303579z | *Nano Lett.* 2012, 12, 6005−6011

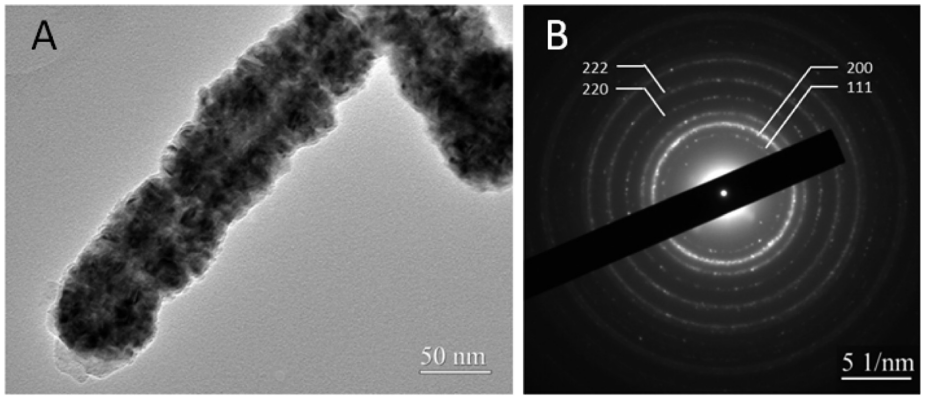

Figure 1. TEM image of nickel-coated TMV1cys after heat treatment at 300 °C for 1 h.

nickel coating via electroless plating due to the strong covalent-like interactions between the thiol group of cysteine and metal ions.[18,19] These surface-assembled high aspect ratio TMV nanostructures represent ideal 3D current collectors that we theorized could be used to reduce the transport distance for a photon-excited charge carrier from the surrounding photoactive material. They also expand the available surface area for photon absorption to increase the water electrolysis reactions. More importantly, by carefully choosing the distance between these virus embedded nanorod structures, we show significant suppression of light reflection and hence improved photon utilization when the spacing between nanorods is shorter than the wavelength of the majority of incident photons.

For the demonstration of this concept, a CuO system with a band gap of 1.4−1.8 eV[21] was chosen for both its broad solar absorption and sufficient energy for splitting water. One of the main limitations of the CuO system is the fast recombination of photon generated charge carriers. In our previous studies,[22] under AM1.5G with 1 sun irradiation, nanosized CuO particles successfully increased the photocurrent density up to 1.20 mA/cm^2 by reducing the possible recombination of charge carriers in the large CuO particle itself.[23] In addition, porous CuO thin film electrodes were introduced to further reduce the charge carrier transport distance within the electrode/electrolyte surface, enhancing water splitting and increasing the photocurrent density to 1.20−1.58 mA/cm^2[24,25] over previous reports that showed photocurrent densities of 0.08−0.44 mA/cm^2.[26,27] However, during these processes, multiple steps were needed for photocathode preparation; that is, the nanoparticles were produced first and then spin-coated to form the film followed by an annealing treatment. With each high-temperature heat treatment, particle growth can be expected, potentially lowering efficiency.

Magnetron sputter deposition thus provides a route to produce CuO particles with a small crystallite size and with the flexibility to deposit films on many different kinds of nanostructures. Furthermore, sputter deposition can be used to produce micro and nanostructural multilayers with different monolayer thicknesses.[28] Sputtering can be used for the deposition of CuO because of its ability to produce evenly dispersed, low-resistance thin films.[29] Here, we demonstrated that an ITO coated TMV1cys template can be used as a current collector for a 3D nanocrystalline CuO photocathode deposited by sputtering. This approach combines the advantages of both small particles, with lower charge carrier recombination rates and short charge carrier transport distance, with the antireflection nature of the structure. Thus, we obtain long carrier lifetimes and can efficiently utilize incident photons to significantly increase photocurrent density.

Virus Template Current Collector. The TMV1cys was self-assembled onto gold-coated ITO/glass substrates via electrostatic interactions between gold and the genetically modified cysteine residues on the amino-terminus. Nickel deposition was done by electroless plating, and a heat treatment at 300 °C for 1 h was applied. The TEM image of TMV1cys structured template nanorods is shown in Figure 1A. The thickness of the nickel coated TMV1cys after heat treatment at 300 °C for 1 h in air was estimated to be about 20 nm and thus gave about 70 nm for the overall diameter of the Ni nanorods. It can be seen in Figure 1B that the nickel oxide (NiO) is crystalline.

Sputter deposition of 4 min produced a thickness of ∼60 nm ITO while a 15 min exposure was found to produce a thickness of ∼520 nm CuO. The image of one sputter coated virus nanorod is shown in Figure 2 along with a line scan EDS

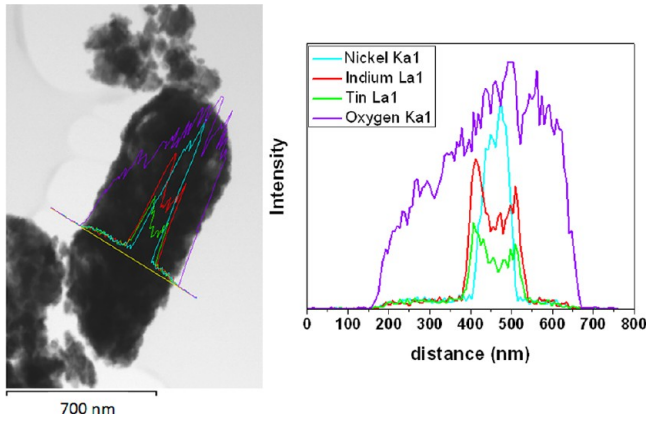

Figure 2. TEM image of a CuO/ITO/NiO nanowire with 15 and 4 min sputter deposition of CuO and ITO and sintered at 450 °C for 1 h.

analysis for the intensity of different elements, that is, Ni, In, Sn, and O, based on the position. A strong signal of nickel from NiO was found in the center of the rod, surrounded by indium and tin from the ITO layer. The outer diameter of the ITO layer was estimated to be 130 nm. Because of the TEM copper grid, the oxygen signal was chosen to demonstrate the CuO concentration at the outermost layer, and this layer was demonstrated to be CuO by XRD as shown in Figure 3. The uniform ITO and CuO deposition indicate the relatively

dx.doi.org/10.1021/nl303579z | Nano Lett. 2012, 12, 6005−6011

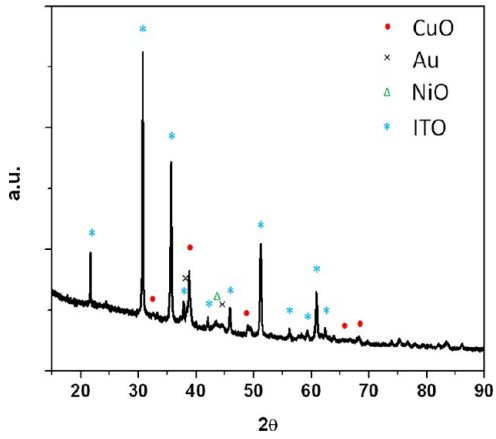

Figure 3. XRD for the film of CuO/ITO/NiO-TMV1cys/Au/ITO-glass.

vertical orientation of the virus on the gold surface because of the thiol-gold interaction. Specifically, the location of the 1cys genetic modification within the virus coated protein is such that the thiol group of the cysteine residue is surface accessible only at one end of the virus rod. This configuration promotes the vertical surface attachment of these viruses.[19]

Film morphology is known to affect the efficiency of solar cell performance through changing the degree of light reflection,[14] charge transport distance,[9] and total surface area.[25] By varying the density of virus deposited on the substrate, the total surface area can be increased up to a factor of 13 over a planar surface.[18] An increase in the density of surface assembled TMV1cys particles was observed between the range of 10^{-4} and 10^{-1} mg/mL. Based on the image analysis of the SEM micrographs as shown in Figure 4, the densities of the deposited TMV1cys particles were 44 ± 8 per 100 μm^2 and 228 ± 25 per 100 μm^2 for TMV1cys concentrations of 10^{-4} and 10^{-3} mg/mL, respectively, while the TMV1cys concentration of 10^{-2} and 10^{-1} gave densities of 403 ± 37 per 100 μm^2 and 610 ± 56 per 100 μm^2, respectively. The average distance between virus particles was found to be 1200 and 500 nm for TMV1cys concentrations of 10^{-4} and 10^{-3} mg/mL, respectively. For more concentrated conditions, viruses tended to have different degrees of overlap between one another. In addition, the surface assembled virus rods have an average length of 600 nm which is about twice the length of a single virus.[30] This length represents the end-to-end alignment of TMV1cys particles that occurs during the self-assembly process in the solution.[15]

Photoelectrochemical Study of CuO Electrodes. The PEC results of CuO photocathode standards sputtered at thicknesses of 170 nm (5 min), 520 nm (15 min), and 1030 nm (30 min) on plain ITO glass substrates are shown in Figure 5. An onset of photocurrent at 0.1 V vs Ag/AgCl was shown for all electrodes, and the photocurrent density for all electrodes showed only a small differences with an applied bias voltage more positive than −0.2 V vs Ag/AgCl. Once the bias voltage passed −0.2 V, the increase in photocurrent density was found for the sample with the virus patterned current collectors. This is likely due to the higher concentration of generated charge carriers and the integrated current collectors providing a more direct path to the contact electrode, thus limiting recombination.

A detailed comparison of photocurrent densities is tabulated in Table 1. The sample ID starting with "a" represents the CuO

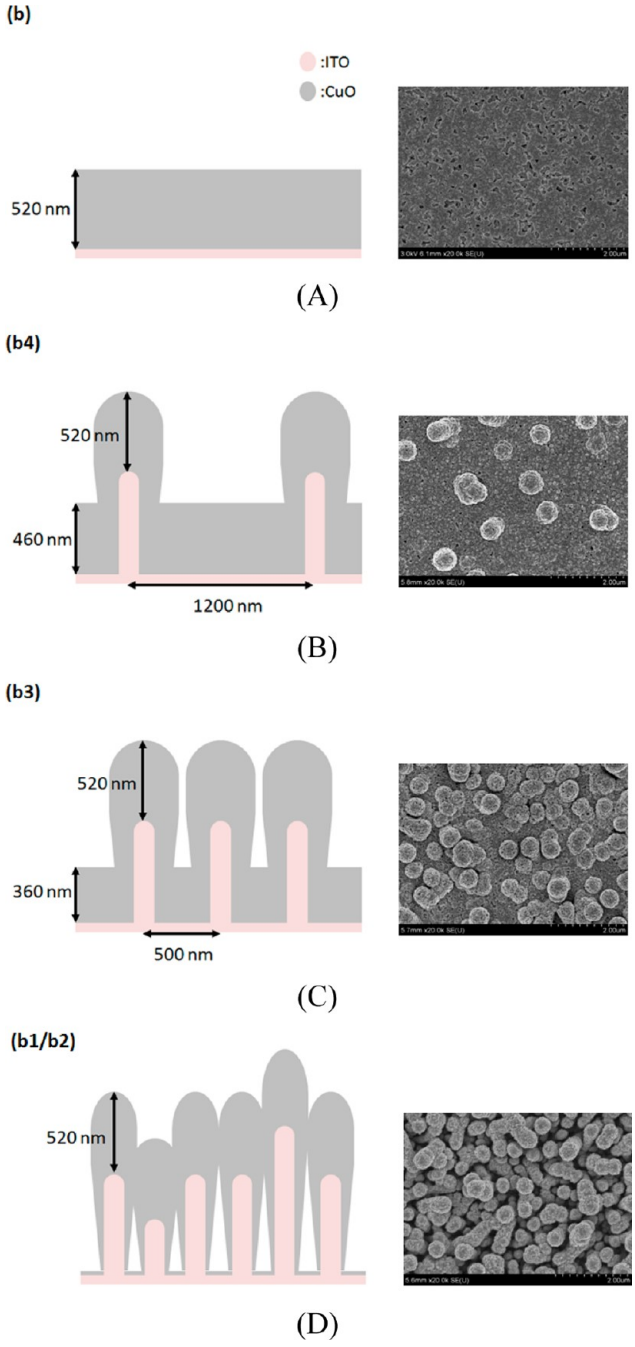

Figure 4. TMV concentration effects on the charge transport distance to the current collector and SEM micrographs for the surface morphology of 15 min CuO sputter deposition on different TMV1cys concentrations of prepared template current collector: (A) plain substrate, (B) 10^{-4} mg/mL, (C) 10^{-3} mg/mL, (D) 10^{-2} mg/mL and 10^{-1} mg/mL.

with thickness of 170 nm, "b" for 520 nm, and "c" for 1030 nm. The number in the sample ID represents the corresponding TMV1cys concentration; that is, a2 means CuO thickness of 170 nm and TMV1cys concentration of 10^{-2} mg/mL, while a3 has concentration of 10^{-3} mg/mL. The highest photocurrent density occurred at a CuO thickness of 520 nm. This half micrometer thickness was also observed to be optimal for other CuO photocathodes in PEC applications.[22] It is not difficult to explain the existence of an optimal thickness for the film because the thicker the layer, the higher the resistance of the

dx.doi.org/10.1021/nl303579z | Nano Lett. 2012, 12, 6005−6011

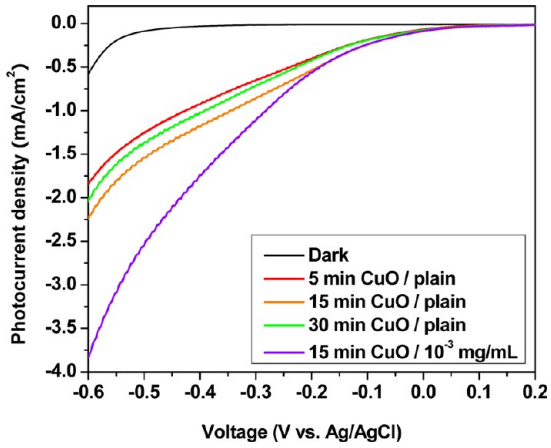

Figure 5. PEC performance of CuO deposited on plain substrates for the sputter deposition time of 5, 15, and 30 min along with a 15 min CuO deposition on TMV1cys patterned substrate.

Table 1. PEC Results Based on Different CuO Thickness and TMV1cys Concentrations

sample ID	CuO thickness (nm)	TMV1cys concentration[a] (mg/mL)	photocurrent density[b] (mA/cm^2)
(a)	170	0	1.50
(b)	520	0	1.80
(c)	1030	0	1.55
(a1)	170	10^{-1}	1.85
(a2)	170	10^{-2}	2.50
(b1)	520	10^{-1}	2.00
(b2)	520	10^{-2}	2.70
(b3)	520	10^{-3}	3.15
(b4)	520	10^{-4}	2.55
(c1)	1030	10^{-1}	2.05
(c2)	1030	10^{-2}	2.50
(c3)	1030	10^{-3}	2.75

[a]TMV1cys concentration in solution. [b]At a bias voltage of −0.55 V vs Ag/AgCl.

film, increasing the chance for charge carrier recombination. Meanwhile, a thicker layer absorbs more incident light and leads to a higher solar irradiation usage. However, a much thicker layer is not necessary because the light penetration depth in CuO for photon energy larger than the bandgap is 150−200 nm.[22] As a result, a film with a thickness of 450−600 nm is sufficient enough to absorb more than 95% of the light.

Introducing the virus-assembled current collector caused the photocurrent densities to increase for all conditions. Additionally, the introduction of virus templated current collectors helped decrease the charge transport distance and thus increased the photocurrent density. However, an interesting phenomenon was found in that the photocurrent density increased with decreasing virus concentration except for the sample (b4), the lowest TMV1cys concentration tested in this experiment. For the detailed illustration of the phenomenon, a scale cross-section cartoon of the samples with corresponding SEM micrographs is given in Figure 4. In Figure 4, CuO was sputtered on the substrates with various concentrations of virus-assembled current collectors, as noted on the top-left corner, for 15 min (520 nm on that flat surface and on top of the current collector). In Figure 4A, sample (b) with 520 nm CuO deposited on a plain ITO substrate showed a 1.8 mA/cm^2 photocurrent density at a bias voltage of −0.55 V vs Ag/AgCl. For sample (b4), with a TMV1cys concentration of 10^{-4} mg/mL, which corresponds to an average distance of ∼1200 nm between the virus-assembled current collectors, the average CuO thickness to was observed to be 460 nm on the area without virus deposited. This might be due to the vertical current collectors serving as geometrical obstacles, that is, shadowing effects, during the sputter deposition. Comparing these two samples, one can see that the shorter charge carrier transport distance was evident in the virus-assembled 3D current collectors, providing more than one direction for the charge carriers to be collected. The photon excited charge carriers on the top surface of the film do not have to go through all 520 nm to be safely separated as in sample (b); on the contrary, the excited charge carriers can find the shorter distance to either the back ITO contact or the 3D ITO current collectors and thus increase the possible lifetime of the charge carriers. Also, the introduction of the virus template provided more surface area.

The highest photocurrent density of 3.15 mA/cm^2 at a bias voltage of −0.55 V vs Ag/AgCl (shown in Figure 5) was achieved at a TMV1cys concentration of 10^{-3} mg/mL (sample b3), which corresponded to an average distance of 500 nm between virus current collectors. Similarly, due to the geometrical obstacles, the thickness of CuO at the area without virus deposition decreased to 360 nm. The highest photocurrent density found in this sample might be due to the shortened charge carrier transport distance of less than or equal to 500 nm, which was shown to be the optimal thickness for the intrinsic CuO samples.[22] In addition, the sample had enough CuO thickness for absorbing solar energy throughout the entire sample. However, as the TMV1cys concentration was further increased to 10^{-2} mg/mL and 10^{-1} mg/mL, samples (b2) and (b1), the highly concentrated virus templates were no longer available for the uniform deposition of the CuO by sputtering. Only a small amount of CuO was deposited on the bottom of the film, that is, on the back ITO contact. Instead, most of the CuO was deposited on the top of the current collectors leaving significant amount of empty space at the bottom of the samples. Because of this situation, the effect of shortening the charge carrier transport distance was not as apparent when compared to the plain substrate. As shown in Table 1, the photocurrent densities for sample (b1) displayed only a 10% increase compared to the plain substrate. The difference between samples (b1) and (b) can be further explained by the slightly increased surface area and the surface roughness of (b1) since the TMV1cys can self-align into different lengths, that is, 600 nm for two viruses and 900 nm for three viruses. This also reduced charge carrier transport distance as shown in Figure 4D.

Based on virus template concentrations of 10^{-2} mg/mL, the CuO was sputtered at different thicknesses, that is, (a2) 5 min for 170 nm, (b2) 15 min for 520 nm, and (c2) 30 min for 1030 nm. This yielded a very different morphology of the films as shown in Figure 6. The average outer diameters of each of the CuO rods increase from 220 to 450 nm and 710 nm, and the detailed construction of each CuO rods is illustrated in Figure 7. As seen in Figures 6 and 7, a uniform rod-like shape was found for the CuO sample sputtered for 5 min, but as sputtering time increased, thicker CuO deposition on the head resulted from the reduced access to the base of the virus nanorods. Based on these samples, the photocurrent density increased from 2.5 mA/cm^2 for (a2) to 2.7 mA/cm^2 for (b2),

dx.doi.org/10.1021/nl303579z | Nano Lett. 2012, 12, 6005−6011

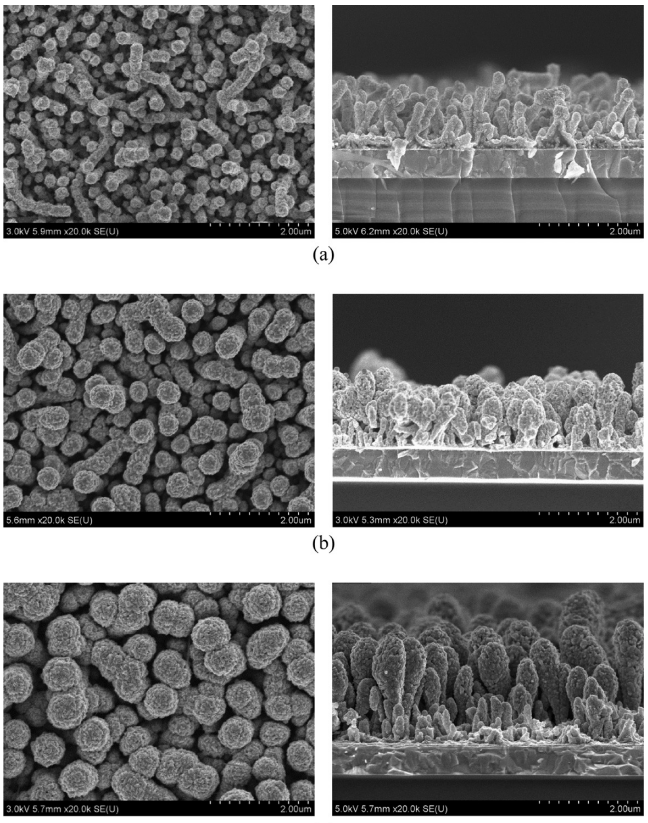

Figure 6. SEM image of virus solution at 10^{-2} mg/mL and sputtering coated with 4 min ITO and various deposition time for CuO: (a) 5 min, (b) 15 min, and (c) 30 min.

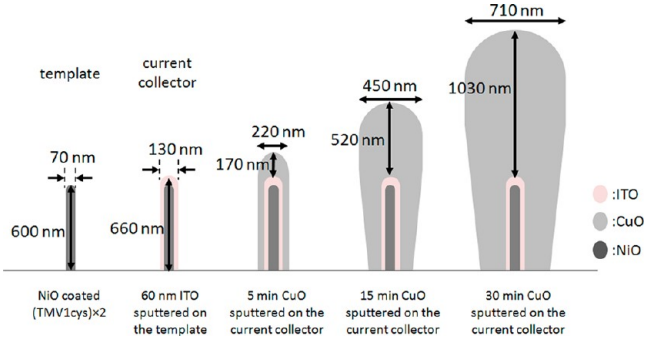

Figure 7. Illustration of the detail construction of virus template, current collector, and each CuO rod at different CuO deposition thicknesses.

but it decreased back to 2.5 mA/cm^2 while increasing the CuO thickness to 1030 nm for (c2) at bias voltage of −0.55 V vs Ag/AgCl as shown in Table 1. This further confirmed the importance of the CuO film thickness to the photocurrent density.

Light and Solid Phase Interactions. When light hits the interface between materials with different refractive indices, a significant portion of it is reflected. With the nanorod surface structure, a graded-refractive index layer was formed, and light experienced a gradual refractive change, reducing reflection associated loss. A comparison of the effect of the surface structure of the samples b, b1, b2, b3 and b4 on light reflection is shown in Figure 8. The mirror-like smooth and light reflecting surfaces were found for samples with TMV1cys

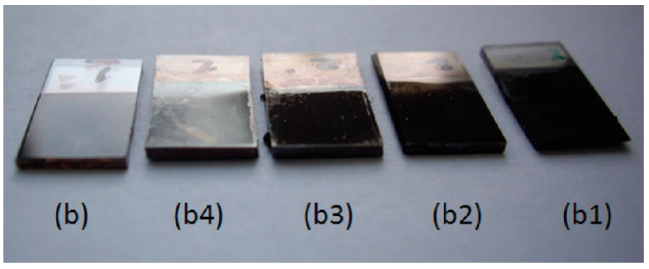

Figure 8. Appearance of samples with 520 nm CuO deposited on different substrates: (b) flat substrate with mirror-like surface, (b4) virus patterned substrate with structure period more than 500 nm, (b3) to (b1) virus patterned substrate with patterned period less than 500 nm which suppresses the light reflection.

concentration less than or equal to 10^{-4} mg/mL (b and b4). However, as the TMV1cys concentration increased to 10^{-3} mg/mL (b3), an antireflecting surface was formed which might be explained by the increased surface roughness and the decreased light reflectance, which can be observed visually. The reflectance of these samples was further quantitatively studied (Figure 9). Light reflectance decreased from 13% to 3% over a wavelength range of 200−600 nm. When the concentration was further increased, there was no apparent difference in reflectance.

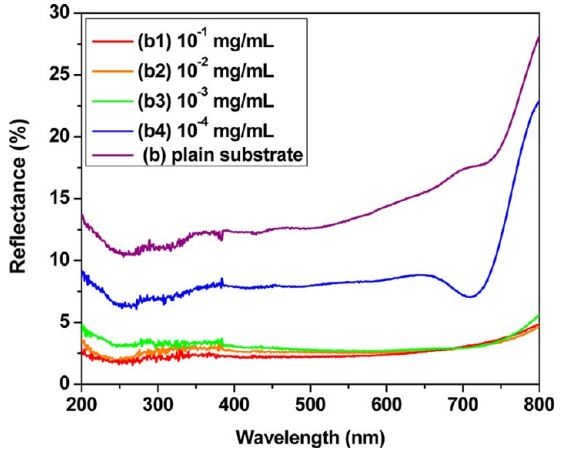

Figure 9. Reflectance of samples with 15 min CuO deposited on different TMV1cys concentration substrates.

Finite difference time domain (FDTD) simulations of the optical fields (Figure 10) are in good agreement with the reflectance data of Figure 9. For a concentration of 10^{-4} mg/mL, the average spacing between TMV1cys structures is >1 μm. For computational simplicity, it was assumed that the structures form a periodic array based on the average spacing between the structures. For a concentration of 10^{-3} mg/mL, the average spacing is ∼540 nm, and the effect of the periodicity on the simulation can be seen as an enhancement of the reflectivity between 400 and 470 nm as shown in Figure 10b. The enhancement or suppression in the reflectivity data between 700 and 800 nm is a thin-film interference effect and depends on the thickness of the CuO layer (see Supporting Information). Despite the complexity of the fabricated structure, this simple model describes the data well.

Photocurrent Density Comparison of Different Systems. The 3D virus-patterned current collectors achieved

dx.doi.org/10.1021/nl303579z | *Nano Lett.* 2012, 12, 6005−6011

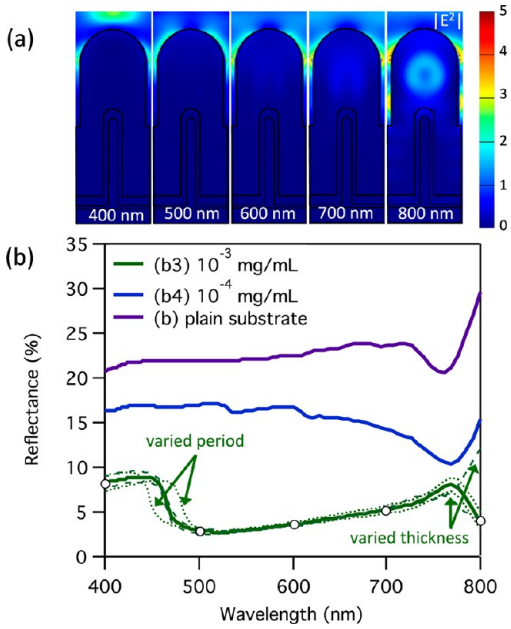

Figure 10. Electromagnetic simulation results for various TMV1cyc concentrations. (a) Cross-section showing the *E*-field intensity with an average TMV1cyc spacing of 540 nm. Each panel represents the field intensity at a specific wavelength, ranging from 400 to 800 nm. (b) Simulated reflectance data for various TMV1cyc concentrations. Dotted lines show that small perturbations in the periodicity (520–560 nm) affect the resonance that occurs for wavelengths around 450 nm. Dashed lines show that the thin-film interference effect between 700 and 800 nm varies with CuO layer thickness (ranging from 420 to 500 nm). Solid white circles correspond to the wavelengths depicted in a.

significantly higher photocurrent densities as compared to other CuO photocathode systems previously reported in the literature[22,24−27,31,32] and are tabulated in Table 2. In this study, the highest photocurrent density was found to be 3.15 mA/cm^2 under 1 sun irradiation (AM1.5G, 1000 W/m^2). This is two to three times higher than our previously reported nanoparticle systems[22,24,25,32] and about an order of magnitude higher than another reported study[26] where a much higher incident light intensity, 8100 W/m^2, was applied. This work demonstrates the effectiveness of composite nanosized 3D current collectors that also function as antireflecting surfaces to further enhance photoelectrochemical cell efficiency.

In conclusion, 3D patterned current collectors were successfully prepared by the self-assembly of TMV1cys on gold coated substrates followed by ITO sputtering deposition. This design likely reduces charge transport distance. In addition, an assembled surface structure with a periodicity of ~500 nm, that is, a TMV1cys concentration at 10^{-3} mg/mL, was demonstrated to suppress light reflection from 13% down to 3% and increase the efficient utilization of incident photons. Furthermore, sputter deposition of CuO at a thickness of 520 nm on the virus-patterned current collectors was demonstrated to produce the highest photocurrent density, that is, 3.15 mA/cm^2, yet reported for nanosized CuO. These results represent the novel integration of bioderived nanoparticles into a photochemical CuO system to achieve a shortened charge carrier transport distance and reduced sample reflectance. Combined with the simplicity of the TMV surface assembly and sputter coating processes, this strategy makes an attractive means to enhance hydrogen generation for use in a number of applications.

■ ASSOCIATED CONTENT

Supporting Information

Detailed synthesis and measurement methods. This material is available free of charge via the Internet at http://pubs.acs.org.

■ AUTHOR INFORMATION

Corresponding Author

*Tel.: 3014051917. E-mail address: sehrman@umd.edu.

Notes

The authors declare no competing financial interest.

■ ACKNOWLEDGMENTS

The authors acknowledge support from National Science Foundation (NSF) DMR 0806610, Dr. Peter Zavalij for performing XRD, Dr. Li-Chung Lai for helping on the STEM, and the Maryland NanoCenter and its NispLab. The NispLab is supported in part by the NSF as a MRSEC Shared Experimental Facility. Jillian Epstein's work was supported by the NSF MRSEC REU, Grant No. DMR-0520471 at the University of Maryland. Jeremy Munday received partial support from a Minta Martin Award.

■ REFERENCES

(1) Yilanci, A.; Dincer, I. *Prog. Energy Combust.* **2009**, *35*, 231.
(2) Turner, J.; Sverdrup, G.; Mann, M.; Maness, P.; Kroposki, B.; Ghirardi, M.; Evans, R.; Blake, D. *Int. J. Energy Res.* **2008**, *32*, 379.
(3) Fujishima, A.; Honda, K. *Nature* **1972**, *238*, 37.
(4) Barborini, E.; Conti, A.; Kholmanov, I.; Piseri, P.; Podestá, A.; Milani, P.; Sancrotti, M. *Adv. Mater.* **2005**, *17*, 1842.
(5) Grätzel, M. *Nature* **2001**, *414*, 338.
(6) Khaselev, O.; Turner, J. *Science* **1998**, *280*, 425.
(7) Hensel, J.; Zhang, J. *Int. J. Nanopart.* **2011**, *4*, 95.
(8) Harris, L. *Annu. Rev. Mater. Sci.* **1978**, *8*, 99.
(9) Kongkanand, A.; Dominguez, R.; Kamat, P. *Nano Lett.* **2007**, *7*, 676.

Table 2. Photocurrent Density of CuO Photocathodes in Different Systems

system	light source	incident power density (W/m^2)	bias voltage (V)	photocurrent density (mA/cm^2)	reference
CuO	150 W solar simulator	1000	−0.55 vs Ag/AgCl	3.15	this study
CuO	500 W xenon lamp		−0.2 vs Ag/AgCl	0.08	27
CuO	150 W xenon arc lamp		−0.5 vs SCE	2.2	31
CuO	150 W solar simulator	1000	−0.55 vs Ag/AgCl	1.20	22
CuO	150 W solar simulator	1000	−0.55 vs Ag/AgCl	1.20	24
CuO	150 W solar simulator	1000	−0.55 vs Ag/AgCl	1.58	25
2 atom % Li-CuO	150 W xenon arc lamp	8100	−0.4 vs SCE	0.44	26
2 atom % Li-CuO	150 W solar simulator	1000	−0.55 vs Ag/AgCl	1.69	32

(10) Faglia, G.; Vomiero, A.; Sberveglieri, G. *SPIE* **2009**, DOI: 10.1117/2.1201001.002531.
(11) Li, Y.; Zhang, J. *Laser Photonics Rev.* **2012**, *4*, 517.
(12) Qiu, Y.; Yan, K.; Deng, H.; Yang, S. *Nano Lett.* **2012**, *12*, 407.
(13) Cho, I. S.; Chen, Z.; Forman, A. J.; Kim, D. R.; Rao, P. M.; Jaramillo, T. F.; Zheng, X. *Nano Lett.* **2011**, *11*, 4978.
(14) Zhu, J.; Yu, Z.; Fan, S.; Cui, Y. *Mater. Sci. Eng. R* **2010**, *70*, 330.
(15) Shenton, W.; Douglas, T.; Young, M.; Stubbs, G.; Mann, S. *Adv. Mater.* **1999**, *11*, 253.
(16) Fowler, C.; Shenton, W.; Stubbs, G.; Mann, S. *Adv. Mater.* **2001**, *13*, 1266.
(17) Dujardin, E.; Peet, C.; Stubbs, G.; Culver, J.; Mann, S. *Nano Lett.* **2003**, *3*, 413.
(18) Royston, E.; Ghosh, A.; Kofinas, P.; Harris, M.; Culver, J. *Langmuir* **2008**, *24*, 906.
(19) Chen, X.; Gerasopoulos, K.; Guo, J.; Brown, A.; Wang, C.; Ghodssi, R.; Culver, J. *ACS Nano* **2010**, *4*, 5366.
(20) Tseng, R.; Tsai, C.; Mai, L.; Quyang, J. *Nat. Nanotechnol.* **2006**, *1*, 72.
(21) Ghosh, S.; Avasthi, D.; Shah, P.; Ganesan, V.; Gupta, A.; Sarangi, D.; Assmann, W. *Vacuum* **2000**, *57*, 377.
(22) Chiang, C. Y.; Aroh, K.; Franson, N.; Satsangi, V.; Dass, S.; Ehrman, S. *Int. J. Hydrogen Energy* **2011**, *36*, 15519.
(23) Jeong, Y.; Choi, G. J. *Phys. Chem. Solids* **1996**, *57*, 81.
(24) Chiang, C. Y.; Shin, Y.; Aroh, K.; Ehrman, S. *Int. J. Hydrogen Energy* **2012**, DOI: 10.1016/j.ijhydene.2012.02.049.
(25) Chiang, C. Y.; Chang, M.; Liu, H. S.; Tai, C.; Ehrman, S. *Ind. Eng. Chem. Res.* **2012**, *51*, 5207.
(26) Koffyberg, F.; Benko, F. *J. Appl. Phys.* **1982**, *53*, 1173.
(27) Nakaoka, K.; Ueyama, J.; Ogura, K. *J. Electrochem. Soc.* **2004**, *151*, C661.
(28) Petrantoni, M.; Rossi, C.; Salvagnac, L.; Conedera, V.; Esteve, A.; Tenailleau, C.; Alphonse, P.; Chabal, Y. *J. Appl. Phys.* **2010**, *108*, 084323.
(29) Parretta, A.; Jayaraj, M.; Di Nocera, A.; Loreti, S.; Quercia, L.; Agati, A. *Phys. Status Solidi A* **1996**, *155*, 399.
(30) Chen, X.; Gerasopoulos, K.; Guo, J.; Brown, A.; Wang, C.; Ghossi, R.; Culver, J. *Adv. Funct. Mater.* **2011**, *21*, 380.
(31) Chauhan, D.; Satsangi, V.; Dass, S.; Shrivastav, R. *B. Mater. Sci.* **2006**, *29*, 709.
(32) Chiang, C. Y.; Shin, Y.; Ehrman, S. *J. Electrochem. Soc.* **2012**, *159*, B227.